AIAA JOURNAL
Vol. 48, No. 9, September 2010

Computation of Wall-Pressure Spectra from Steady Flow Data for Noise Prediction

S. Remmler,* J. Christophe,† and J. Anthoine‡
von Karman Institute for Fluid Dynamics, 1640 Rhode-St-Genèse, Belgium
and
S. Moreau§
Université de Sherbrooke, Sherbrooke, Québec J1K 2R1, Canada

DOI: 10.2514/1.J050206

A method is proposed to calculate the trailing-edge broadband noise emitted from an airfoil, based on a steady Reynolds-averaged Navier–Stokes solution of the flowfield. For this purpose, the pressure spectrum on the airfoil surface near the trailing edge is calculated using a statistical model from the Reynolds-averaged Navier–Stokes mean velocity and turbulence data in the airfoil boundary layer. The obtained wall-pressure spectrum is used to compute the radiated sound by means of an aeroacoustic analogy, namely, Amiet's theory of airfoil sound. The statistical model for wall-pressure fluctuations is validated with two test cases from the literature, a boundary layer with an adverse pressure gradient, and a flat plate boundary layer without a pressure gradient. The influence of specific model assumptions is studied, such as the convection velocity of pressure-producing structures and the scale anisotropy of boundary-layer turbulence. Furthermore, the influence of the Reynolds-averaged Navier–Stokes simulation on the calculated spectra is investigated using three different turbulence models. The method is finally applied to the case of a Valeo controlled-diffusion airfoil placed in a jet wind tunnel in the anechoic facility of École Centrale de Lyon. Reynolds-averaged Navier–Stokes solutions for this test case are computed with different turbulence models, the wall-pressure spectrum near the trailing edge is calculated using the statistical model, and the radiated noise is computed with Amiet's theory. All intermediate results of the method are compared with experimental data.

Nomenclature

b	=	airfoil span
C_μ, C_L, C_η, C_m	=	turbulence model constants
c	=	airfoil chord length
c_p	=	pressure coefficient
c_0	=	speed of sound
K	=	turbulent kinetic energy
k_i	=	wave number components
L	=	turbulence length scale
L_p	=	sound pressure level
l_m	=	Prandtl mixing length
p	=	local instantaneous pressure
q	=	dynamic pressure
R_r	=	observer distance from trailing edge
Re	=	Reynolds number
t	=	time
U_c	=	convection velocity of pressure-producing structures
U_τ	=	wall friction velocity
U_∞	=	freestream velocity
u_i	=	local instantaneous velocity components
$\langle u \rangle$	=	time average of u
u'	=	fluctuations of u
u^+	=	nondimensional velocity, $\langle u_1 \rangle / U_\tau$
$\bar{u}'$	=	root-mean-square value of fluctuations
x_i, $\hat{x}_i$	=	space coordinates
y^+	=	nondimensional wall distance, $x_2 U_\tau / \nu$
α	=	ratio of streamwise to spanwise turbulent length scales
β	=	ratio of vertical fluctuations to total kinetic energy
γ	=	angle between global x diriection and local wall tangent
Δ_{int}	=	integral error of calculated pressure spectrum compared with experimental spectrum
δ	=	boundary-layer thickness (99.5% U_∞)
δ_{ij}	=	Kronecker symbol
δ^*	=	displacement thickness
ε	=	turbulent dissipation
θ	=	momentum thickness
θ_r	=	observer angle against horizon
κ	=	von Karman constant, 0.41
Λ	=	velocity correlation length scale
μ	=	dynamic viscosity
ν	=	molecular viscosity
ρ	=	density
τ	=	shear stress
τ_{nd}	=	nondimensional time
Φ	=	wall-pressure frequency spectrum
ϕ	=	wall-pressure wave number spectrum
ω	=	angular frequency
ω	=	specific dissipation rate (in k-ω turbulence models)

Presented as Paper 2010-4000 at the 16th AIAA/CEAS Aeroacoustics Conference, Stockholm, Sweden, 7–9 June 2010; received 10 September 2009; revision received 28 May 2010; accepted for publication 28 May 2010.

*Diploma Course Student; currently Ph.D. Candidate, Technical University of Munich, Lehrstuhl für Aerodynamik, Boltzmannstrasse 15, 85748 Garching, Munich, Germany.

†Ph.D. Candidate, Environmental and Applied Fluid Dynamics Department, Chaussée de Waterloo 72; christju@vki.ac.be. Member AIAA.

‡Associate Professor, Environmental and Applied Fluid Dynamics Department, Chaussée de Waterloo 72; currently ONERA, Propulsion Laboratory, Midi-Pyrenees Center, Mauzac, France. Senior Member AIAA.

§Professeur Agrégé, Mechanical Department of Engineering, 2500 Boulevard de l'Université.

Introduction

BROADBAND noise generated by wall-bounded flows is subject to an increasing interest in the aeronautic industry. Because of the strong reduction of jet noise in recent aircraft engines, the sound

reduction of landing and approaching aircraft is more and more limited by airframe noise, especially from landing gears, wings, and high-lift devices [1,2]. In many kinds of fans, from large aeroengine turbofans down to low-speed ventilators, broadband noise due to the interaction of blades with turbulent flow is a significant source of sound and can even become dominant in many configurations [3–5]. The same applies to wind turbines, which generate very unpleasant noise, limiting their acceptance to inhabited areas [6–8]. Ventilation and cooling systems are installed, increasingly, both in residential and office buildings to increase the energetic efficiency, but reduction of the produced noise raises new challenges for the heating, ventilation, air-conditioning, and refrigeration (HVACR) industry [9,10]. Finally, in the automotive industry, noise generated aerodynamically is also a big issue, especially in terms of passenger comfort and general appreciation of the product. The car ventilation system generates a lot of noise [11,12], and the noise from the interaction of the car body with turbulent and partly separated flow becomes significant at high cruising speeds beyond 100 km/h [13,14].

Sound generated aerodynamically can be calculated by means of aeroacoustic analogies, all based on the pioneering work of Lighthill [15,16]. Under the conditions of high Reynolds numbers, small acoustic fluctuations compared with turbulent perturbations, and a sound receiver placed far away from the source region, the acoustical field can be decoupled from the turbulent flowfield. The generated sound field can be calculated from the results of the flow computation. Curle [17] proposed an integral formulation to calculate the sound from turbulent flows over solid surfaces, and the analogy of Ffowcs Williams and Hawkings [18] allows these surfaces to be unsteady and permeable. Both of the latter methods require some knowledge about the unsteady pressure distribution or the equivalent spectrum on the surface caused by the turbulent flow and are mainly applicable for acoustically compact source regions (i.e., for the low-frequency part of the spectrum). Amiet [19] developed a theory for the sound radiation from the trailing edge of a simplified airfoil that also takes into account noncompactness effects. This theory has been extended by Roger and Moreau [20,21] and Roger et al. [22] to take into account the leading edge and its corresponding backscattering effects as well. Christophe et al. [23] also proposed a method to apply Amiet's theory [19] to nonuniform inlet flow, which allowed the treatment of applications like fans and wind turbines.

Moreau et al. [24] used the extended Amiet's [19] theory to predict the noise radiated from a finite-span airfoil. The results were validated by measurements in an open free-jet anechoic wind tunnel at École Centrale de Lyon (ECL) [25]. The necessary turbulent surface-pressure fluctuations near the trailing edge were obtained by large eddy simulations (LES) [24,26]. A good agreement between computations and measurements was found for this rather simple test case, but the method is still far from being applicable to complex industrial problems. The main problem is that, according to Wang et al. [26], acceptable solutions require a high spatial and temporal resolution of the LES, which would mean using grid sizes beyond 500 million cells for this simple test case. Thus, it is certainly not feasible to use LES for a complete fan with twisted and swept blades and a tip clearance. For the prediction of the self-noise of a complete fan, Moreau et al. [27] used a simplified approach, splitting the fan blades into several strips, which are considered to behave exactly like stationary airfoils in the wind-tunnel experiments. In this way, the results of two-dimensional LES computations could be used as source terms for sound generation.

The most important aim in the field of fan noise prediction is the reduction of computational costs while keeping a reasonable accuracy of sound levels and frequency content. Additionally, the prediction method should not be restricted to exactly one type of geometry but have, at least, a certain universality. The most critical part concerning the computational costs is the LES, which may thus be replaced by much cheaper Reynolds-averaged Navier–Stokes (RANS) solutions. The new problem arising from this approach is the necessity to model the surface-pressure spectrum or the unsteady pressure distribution on the blades from the turbulence information.

The problem of wall-pressure fluctuations beneath a turbulent boundary layer was first theoretically treated by Kraichnan [28] in the 1950s. He derived an expression for the pressure fluctuations on the wall dominantly as a function of the mean velocity profile and the two-point correlation of the velocity fluctuation components perpendicular to the wall.

Kraichnan's theory was extended by Lilley and Hodgson [29] and Lilley [30] to also be valid for boundary layers with a pressure gradient in the streamwise direction. Their computations rely strongly on empirical input data, such as the velocity profiles, the velocity fluctuations, and the correlation lengths. Nevertheless, their calculations, at least, predicted the order of magnitude and the qualitative shape of the pressure spectrum.

Panton and Linebarger [31] used empirically determined analytical expressions for velocity, fluctuations, and turbulence length scale as input for the Kraichnan [28] integral. The equation included a fivefold multiple integration, which had to be solved numerically. To handle this multiple dimension problem with reasonable computational costs, the Monte Carlo technique was applied. They showed the effect of pressure gradient and turbulence anisotropy on the wall-pressure spectrum. Furthermore, it was shown that the low-frequency part of the spectrum is dictated by the turbulence in the outer region of the boundary layer, while the high frequencies are dominated by the inner and middle layers.

The next logical step with availability of powerful RANS solvers was to switch from purely empirical input data to case-dependent computational input. Lee et al. [32] showed that the principal approach of Kraichnan [28] was also applicable to more complex nonequilibrium-type boundary layers, such as the reattachment after a backward-facing step. They used a RANS solution for the prediction of mean velocity and velocity fluctuations and some empirical input for the spectral content of turbulent motion, based on the measurements of Farabee and Casarella [33]. They found a good agreement with a number of experimental results for a wide part of the spectrum.

Rozenberg et al. [34] combined RANS simulations with semi-empirical wall-pressure spectra to compute the noise radiated by an airfoil placed in the open jet of an anechoic wind tunnel by an automotive cooling fan and by an aircraft engine fan.

A different method was recently presented by Glegg et al. [35], who directly related distributions of turbulent kinetic energy in a boundary layer to the wall-pressure spectrum by solving a linearized vorticity equation. They applied their method to a NACA 0012 airfoil and to a rotating fan, and they could predict the self-noise in both cases with satisfying accuracy.

Another approach to derive acoustical source data from steady RANS solutions is the reconstruction of a turbulence field by means of a stochastic method. This can be used for completely three-dimensional flows, including quadrupole noise production, such as turbulent jets. Examples can be found in the work of Bèchara et al. [36] and Golliard et al. [37]. Both used the derived turbulent velocity field as source terms for linearized Euler equations for sound propagation. This approach is suited for complex geometries, including different mechanisms of sound generation; but, on the other hand, it requires much higher computational costs than the described methods based on the ideas of Kraichnan [28].

The present work will concentrate on the use of a statistical model for modeling surface-pressure spectra according to Kraichnan [28], Lilley and Hodgson [29], and Panton and Linebarger [31]. A RANS solver is used to compute the mean flowfield and turbulence quantities, which are then used as input for the statistical model. This method is first validated for two literature cases, a boundary layer with adverse pressure gradient and a boundary layer with zero pressure gradient, for which mean flow and surface-pressure spectrum are known. Next, the method is applied to the well-studied case of a controlled-diffusion (CD) airfoil in a jet wind tunnel, which is a first step toward the prediction of low-speed fan noise [24,25,27,38,39]. The wall-pressure spectrum close to the trailing edge is calculated by means of the statistical model and is used to compute the radiated trailing-edge noise, using the extended Amiet's [19] theory.

Numerical Tools

Steady Flow Simulation

For the computation of the steady flowfield, the commercial solver STAR–CCM+ (version 3.04.008) [40] was used. This is a typical finite-volume solver, and it is widely used for industrial applications, since it is known to provide good convergence and acceptable accuracy for many engineering applications. The partial differential equations are discretized using a second-order upwind interpolation scheme that, for simple flows, is a good compromise between stability and accuracy. Other computations were also made with FLUENT (version 6.3.26) [41]. Details concerning computational grids and boundary conditions will be found in the descriptions of the single cases.

Three different turbulence models were evaluated in the present study:

1) The K-ω model [42] in the shear stress transport extension [43] is a good choice in many practical applications of wall-bounded flows. It is based on isotropy of turbulent structures and hence requires some additional modeling if wall-normal velocity fluctuations are required.

2) The v^2f model is an extension of the standard K-ε model developed by Durbin [44,45]. An additional set of transport equations is solved for the wall-normal velocity fluctuations $\langle v^2\rangle$ and their production f.

3) In the case of Reynolds stress turbulence models (RSTMs) [46], a transport equation is solved for each of the components of the Reynolds stress tensor and for the turbulent dissipation rate; in total, seven additional equations. The main advantage of RSTM is the completely anisotropic treatment of turbulent motion; the drawbacks are high computational costs and convergence problems due to the stiff system of equations.

All of the computational grids used had a high resolution near the walls to ensure grid-independent solutions [47], so that the viscous sublayer was properly resolved and no additional turbulence wall modeling had to be applied. This was not only helpful to limit the number of assumptions in the RANS computation but also necessary to generate highly resolved velocity information near the wall to model the wall-pressure spectrum accurately.

Modeling of Wall-Pressure Spectra

To derive an equation for the wall-pressure fluctuations caused by a turbulent boundary layer, the incompressible Navier–Stokes equations for a Newtonian fluid are rewritten in the form of a Poisson equation for the pressure. After neglecting viscous terms, assuming high Reynolds number flows, and performing a Reynolds decomposition into mean and fluctuating quantities, the following equation for the pressure fluctuations is obtained:

$$\frac{1}{\rho}\frac{\partial^2 p}{\partial x_i^2} = \underbrace{-2\frac{\partial\langle u_i\rangle}{\partial x_j}\frac{\partial u_j'}{\partial x_i}}_{\mathrm{MT}} \underbrace{-\frac{\partial^2}{\partial x_i \partial x_j}\left(u_i'u_j' - \langle u_i'u_j'\rangle\right)}_{\mathrm{TT}} \tag{1}$$

The right-hand side of this equation is assumed to be known. In the present application, only the mean shear–turbulence interaction term (MT) is considered, while the turbulence–turbulence interaction term (TT) is neglected. According to Kraichnan [28], Lilley and Hodgson [29], and Panton and Linebarger [31], the TT term is only responsible for approximately 5% of the pressure fluctuations at mid and high frequencies but is of higher importance at low frequencies, when $\omega\delta^*/U_\infty \lesssim 0.1$.

It can be assumed that the flow is statistically stationary and homogeneous in streamwise and spanwise directions if the mean velocity and fluctuation are approximately constant within the turbulence length scale. This is the case for many slowly growing boundary layers. With only the wall-normal direction remaining as a free coordinate, the Poisson equation can be solved by means of the Green's function technique (for details, see the paper of Lilley and Hodgson [29]), yielding an explicit expression for the unsteady pressure at the wall:

$$p(\mathbf{x},t)|_{x_2=0} = \frac{\rho}{\pi}\int_{\hat{x}_2>0}\frac{1}{|\mathbf{x}-\hat{\mathbf{x}}|}\frac{\partial\langle u_1\rangle(\hat{\mathbf{x}})}{\partial x_2}\frac{\partial u_2'(\hat{\mathbf{x}})}{\partial x_1}\,\mathrm{d}\hat{\mathbf{x}} \tag{2}$$

which includes an integration over the complete upper half-space of $\hat{\mathbf{x}}$, so the wall pressure at each arbitrary position depends on velocity information in the whole flowfield.

To obtain the pressure spectrum from the preceding expression, Lilley and Hodgson [29] used the following approach. The pressure covariance on the wall for zero time delay can be Fourier-transformed in planes parallel to the wall. Integration over the spanwise wave number component k_3 leads to the final expression for the streamwise wall-pressure wave number spectrum:

$$\phi(k_1) = 8\rho^2 \quad \infty\iint_0^\infty\int \frac{k_1^2}{|k|^2}e^{-|k|(x_2+\hat{x}_2)}S_{22} \times\cdots\frac{\partial\langle u_1\rangle}{\partial x_2}\frac{\partial\langle u_1\rangle}{\partial\hat{x}_2}\,\mathrm{d}x_2\,\mathrm{d}\hat{x}_2\,\mathrm{d}k_3 \tag{3}$$

where $|k| = \sqrt{k_1^2 + k_3^2}$, and S_{22} is the energy spectrum of the vertical velocity fluctuations given by

$$S_{22} = \frac{\bar{u}_2'(x_2)\bar{u}_2'(\hat{x}_2)}{\pi^2}\Lambda^2\int_0^\infty\int R_{22}\cos(\alpha\tilde{k}_1\tilde{r}_1)\cos(\tilde{k}_3\tilde{r}_3)\,\mathrm{d}\tilde{r}_1\,\mathrm{d}\tilde{r}_3 \tag{4}$$

R_{22} corresponds to the velocity correlation coefficient, which has to be modeled, and α accounts for the scale anisotropy of the streamwise structures when compared with the spanwise structures. The integration coordinates and the wave numbers were nondimensionalized with the velocity correlation length scale Λ:

$$\tilde{r}_i = \frac{r_i}{\Lambda}, \qquad \tilde{k}_i = k_i\Lambda, \qquad \tilde{y} = \frac{(x_2-\hat{x}_2)}{\Lambda} \tag{5}$$

where Λ is given by Eq. (7) and is then computed from the Prandtl mixing length, which is dependent on the wall distance, as it will be shown from the second test case of the "Validation of the Statistical Model"section

For the velocity correlation coefficient, the nondimensional expression

$$R_{22} = \left[1 - \frac{\tilde{r}^2}{2\sqrt{\tilde{r}^2+\tilde{y}^2}}\right]e^{-\sqrt{\tilde{r}^2+\tilde{y}^2}}, \qquad \tilde{r}^2 = \tilde{r}_1^2 + \tilde{r}_3^2 \tag{6}$$

proposed by Panton and Linebarger [31] was used. The vertical velocity correlation coefficient R_{22} is only spatially invariant in coordinates scaled with the velocity correlation length scale Λ, which generally is a function of the wall-normal coordinate. The symmetry of R_{22} implies local homogeneity of the turbulence, which was regarded as an acceptable simplification by Panton and Linebarger [31].

The final expression to solve is Eq. (3), which is depending on Eqs. (4–6). It includes an integration over five dimensions (x_2, $\hat{x}_2$, k_3, r_1, and r_3), which is difficult to evaluate with classical integration methods, like trapezoidal integration, due to the propagation of the error between the successive integrations. Discretizing these in sufficiently large domains with acceptable accuracy would require an array exceeding the memory in typical PCs and would take too much time. The computational cost for a Monte Carlo integral is not dependent on the number of integrations and is then more efficient when compared with a trapezoidal integration when the dimension is higher than two (as is the case here, with a dimension of five). Equation (3) was then solved by the help of a Monte Carlo method, using importance sampling for enhancing convergence [31,48]. The pressure power spectral density was calculated at 1000 frequencies, each of them based on 3000 random input data sets. MATLAB (version 7.5.0.338) was used for the computation. One wave number spectrum was calculated within around 90 s of computational time on an Intel Core 2 processor (1.8 GHz). To obtain the frequency spectrum of the pressure $\Phi(\omega)$, Eq. (3) has to be evaluated and transformed using $\omega = k_1U_c$, where $U_c(k_1)$ is the convection velocity of surface-pressure-producing structures in the flow. In other

words, U_c is the velocity with which the pressure footprint, which a turbulent structure generates on the wall, moves along the wall. The dependence of the convection velocity model with the wave number is given in Eqs. (13) and (14) through the parameter k_1. Large structures in the mean will be found far away from the wall and hence move nearly with the freestream velocity. Small structures must be close to the wall to have a significant effect on the wall pressure and then, consequently, move slower if a usual boundary-layer profile is assumed. This indirect dependence of U_c on the wave number is discussed by Panton and Linebarger [31] and Lee et al. [32].

The forestanding expressions require knowledge about the time-averaged flowfield ($\langle u_1 \rangle$, $\bar{u}_2'$, Λ) on a profile in the x_2 direction (wall-normal), which can be obtained from a RANS solution. The quantities α, R_{22}, and U_c cannot be extracted from RANS solutions and thus have to be modeled.

The root mean square of wall-normal velocity fluctuations $\bar{u}_2'$ is usually not provided by RANS solutions unless a RSTM is used. Two-equation turbulence models, such as the K-ε or K-ω models, only provide the turbulent kinetic energy $K = 0.5 \sum \bar{u}_i'^2$, which also includes the streamwise and spanwise fluctuation components. As can be seen from the often-cited measurements of Klebanoff [49], in a zero pressure gradient boundary layer, the composition of K is not constant over the vertical coordinate, so $\bar{u}_i'^2$ are not constant fractions of $2K$ and, instead, an anisotropy factor is defined for each component as $\beta_i = \bar{u}_i'^2/2K$. The factors $\beta_i(x_2)$ are not universal for any kind of boundary layer. However, in the first approximation, the values from the zero pressure gradient boundary layers are also applicable to other equilibrium boundary layers. In the present investigation, $\beta_i(x_2)$ were calculated from a RANS computation of a flat plate boundary layer, using a Reynolds stress transport turbulence model, and then applied to the results of all K-ω computations. The calculated $\beta_i(x_2)$ are shown in Fig. 1. For v^2f and RSTM computations, the wall-normal fluctuations can be calculated directly from the the RANS solution, so no modeling is necessary.

Panton and Linebarger [31] concluded from experimental data that the length scale Λ is approximately 1.5 times the Prandtl mixing length l_m, so

$$\Lambda = 1.5 l_m = 1.5 \sqrt{\frac{-\langle u_1' u_2' \rangle}{|\partial \langle u_1 \rangle / \partial x_2| \cdot (\partial \langle u_1 \rangle / \partial x_2)}} \tag{7}$$

The Reynolds stress $-\langle u_1' u_2' \rangle$ is not computed by most turbulence models, so Eq. (7) cannot be used in those cases. The simplest choice would be following the approach of Prandtl, who estimated the mixing length to $l_m = \kappa x_2$ for $x_2 < 0.22\delta$ and to a constant value of $l_{m,\max} = 0.09\delta$ for $x_2 > 0.22\delta$. The disadvantage of this simple approach is that, for boundary layers other than zero pressure gradient, the estimation is quite poor.

For turbulence models that provide a kinetic energy and a turbulent dissipation, these quantities can be used to calculate the turbulence length scale $L = l_m / C_m$ from

$$L = C_\mu \frac{K^{3/2}}{\varepsilon}, \qquad C_\mu = 0.09 \tag{8}$$

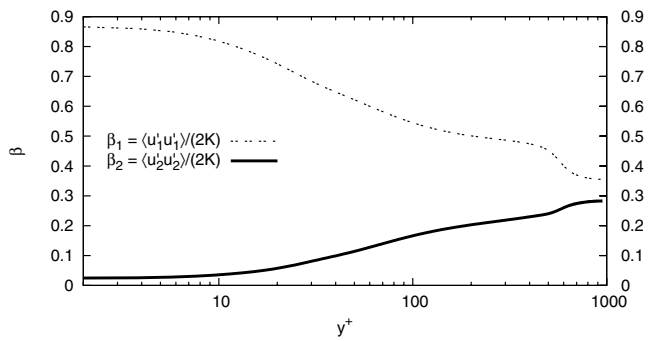

Fig. 1 Turbulence anisotropy factors in a flat plate boundary layer (RANS computation with RSTM at $\mathrm{Re}_{\delta^*} = 1950$).

The numerical values of model constants, such as C_μ, are the default values used in the STAR–CCM+ computations. Equation (8) is used for computations using the RST and K-ω models. Note that, for the latter one, the turbulent dissipation is calculated from $\varepsilon = K\omega$. For the v^2f model of Durbin [45], the length scale is obtained from

$$L = C_L \max\left[\frac{K^{3/2}}{\varepsilon}; C_\eta \left(\frac{\nu^3}{\varepsilon}\right)^{1/4}\right] \qquad C_L = 0.23, \qquad C_\eta = 70.0 \tag{9}$$

C_m is a turbulence model constant. Its value was set to 1.9 for the K-ω and RST models and to 0.65 for the v^2f model.

Amiet's Theory for Airfoil Trailing-Edge Noise

Based on the observation that airfoil trailing-edge noise is basically due to interaction of the turbulent boundary-layer flow with the geometrical discontinuity at the trailing edge, Amiet [19,50] developed a theory that links the radiated sound to the wall-pressure fluctuations close to the trailing edge. The trailing-edge noise is derived by iteratively solving scattering problems at the airfoil edges. The system of partial differential equations that arises at each iteration in this multiple scattering problem is solved by the standard Schwarzschild's solution. The main trailing-edge scattering is first determined by assuming that the airfoil surface extends toward infinity in the upstream direction. Amiet [50] reduced the formulation to this first evaluation and calculated the radiated sound field by integrating the induced surface sources on the actual chord length c and the mockup span L, assuming convection of frozen turbulent boundary-layer eddies past the trailing edge. This provides a first evaluation of the radiation integral I, say $I \simeq I_1$. A leading-edge correction, fully taking into account the finite chord length (second iteration and correction I_2 to I), has been derived by Roger and Moreau [20,21]. The predicted sound field in the midspan plane at a given observer location $\mathbf{x} = (x_1, x_2, 0) = (R_r, \theta_r, z = 0)$ and for a given radian frequency ω (or wave number k) then reads

$$S_{pp}(\mathbf{x}, \omega) = \left(\frac{\sin\theta_r}{2\pi R_r}\right)^2 (kc)^2 \frac{b}{2} |I|^2 \Phi(\omega) l_y(\omega) \tag{10}$$

where Φ is the wall-pressure power spectral density and l_y the spanwise correlation length near the trailing edge. The radiation integral $I = I_1 + I_2$ involving both the freestream velocity U_∞ and the convection speed U_c as parameters is given by Roger and Moreau [21].

In the following section, methods for modeling the wall-pressure spectrum Φ and the convection speed U_c will be presented. For the correlation length l_y, we refer to experimental data for the investigated configuration. This could mean that our method is not standalone, since the parameter l_y is not computed. However, this parameter is directly linked to the use of Amiet's [19] theory, and we could have shown the influence of the choice of the RANS model (k-ϵ, $\cdots$) on the acoustic prediction, which is the objective of the present work, by using the Ffowcs Williams and Hawkings [18] analogy, for which the l_y would not have been raised, instead of the Amiet's theory.

Validation of the Statistical Model

The method is first validated for two literature test cases for which mean flow and surface-pressure spectrum are known. They are not ordered by their complexity but by their purpose for validation of the spectral model. For choosing appropriate models for the empirical quantities α, R_{22}, and U_c, it was necessary to use an experimental database that includes the complete set of flow data (mean velocity, vertical velocity fluctuations, and turbulence length scale) and wall-pressure data. Bradshaw [51] provides these experimental data for the boundary layer with adverse pressure gradient. The second test case was chosen to investigate the influence of the RANS computation on the calculated spectrum. The simplest test case to be imagined for this purpose was a zero pressure gradient boundary layer.

Test Case 1: Boundary Layer with Adverse Pressure Gradient

A first test case was built up by using the published data of Bradshaw [51], who made hot-wire measurements in equilibrium boundary layers with adverse pressure gradients ($U_\infty = 37$ m/s, $\delta = 114$ mm, and $\mathrm{Re}_{\delta^*} = U_\infty \delta^*/\nu = 60,500$). This case was chosen because all necessary input data for the statistical model and the measured wall-pressure spectrum are published, so no RANS computation was required. This allowed testing several models for the unknown parameters without introducing errors through the RANS solution, which was done for the scale anisotropy factor α and the convection velocity of the pressure-producing turbulence structures U_c.

Scale Anisotropy Factor

Panton and Linebarger [31] calculated spectra for $\alpha = 1$, 2, and 3 and found that increasing the anisotropy factor does not change the shape of the spectrum very much, but it increases its level and shifts it to lower wave numbers. The same behavior can be found for the present boundary layer (Fig. 2).

It is reasonable to assume that the scale anisotropy depends on the wave number. Turbulent structures with low wave numbers generally have a higher tendency to strong anisotropy than high wave number structures, which tend more to isotropical behavior. The parameter α was set as follows for the present calculation:

$$\alpha = \begin{cases} 3 & k_1\delta < 1 \\ \text{linear decrease} & 1 \le k_1\delta \le 5 \\ 1 & k_1\delta > 5 \end{cases} \tag{11}$$

to best match the spectrum obtained experimentally (Fig. 2). With this definition of α, the peak position is computed correctly, although the maximum is overestimated by 2 dB. The integral error, characterizing the difference of the whole energy of the calculated pressure spectrum with respect to the experimental spectrum

$$\Delta_{\mathrm{int}} = 10\lg\left(\frac{\int \Phi_{\mathrm{calc}}(\omega)\,\mathrm{d}\omega}{\int \Phi_{\mathrm{exp}}(\omega)\,\mathrm{d}\omega}\right) \tag{12}$$

is 0.8 dB, and the decay at high frequencies matches the experiment quite well. Regarding the low-frequency domain $\omega\delta^*/U_\infty < 0.1$, it should be noted that all available experimental data (including the one quoted) have a very low accuracy in this part of the spectrum due to external noise. Additionally, the computations also have a low accuracy at low frequencies due to the neglect of TT in the model.

Convection Velocity

Three different models for the convection velocity U_c were tested. In the first one, model a, U_c was set to a constant value of $U_c \propto U_\infty$ without any dependence on the wave number, as it was used by Lee et al. [32]. For the second one, model b, an empirical expression

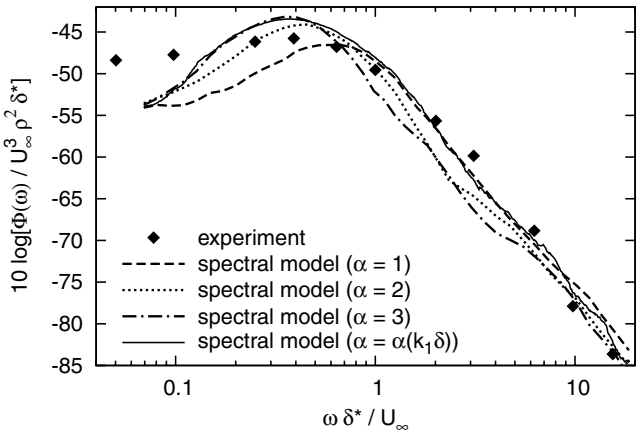

Fig. 2 Calculated wall-pressure spectra for different models of scale anisotropy. Experiment from Bradshaw [51].

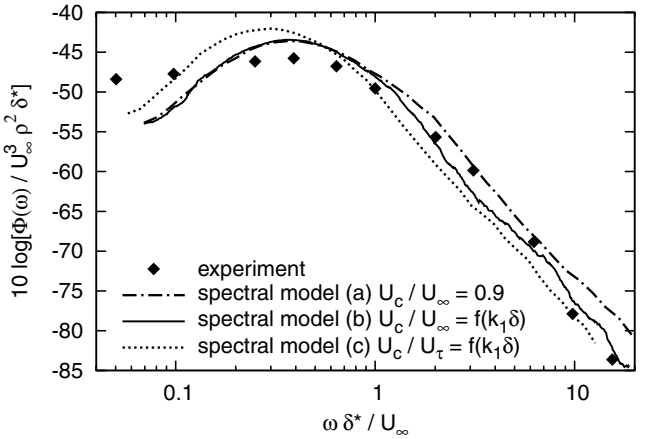

Fig. 3 Calculated wall-pressure spectra for different models of convection velocity. Experiment from Bradshaw [51].

based on the mean flow velocity U_∞ was derived from the measurements of Wills [52]:

$$\frac{U_c}{U_\infty} = 0.92 - \frac{1}{8}\ln(k_1\delta) \tag{13}$$

with $0.55 \le U_c/U_\infty \le 0.9$. The third model, model c, was proposed by Panton and Linebarger [31], who used a law based on the wall friction velocity

$$\frac{U_c}{U_\tau} = -\frac{1}{\kappa}\ln(k_1\delta) + \frac{1}{\kappa}\ln\frac{U_\tau\delta}{\nu} + 5.0 \tag{14}$$

for their computations.

The spectra calculated with each of these three models are plotted in Fig. 3. The influence of the convection velocity model on the calculated spectrum is rather small. Models a and b produce nearly the same spectra, except in the high-frequency range, where model b produces slightly lower values due to the lower convection velocity. The integral pressure fluctuation of model b (+0.8 dB) is thus a bit closer to the experiment than the one of model a (+1.3 dB). The spectrum calculated with model c is shifted to lower frequencies and higher amplitudes, hence the peak is about 2 dB higher, while the integral difference is small as well (+0.9 dB). Thus, model b performs slightly better than the others for this test case.

Test Case 2: Flat Plate Boundary Layer

The second test case, an equilibrium flat plate boundary layer with zero pressure gradient at $\mathrm{Re}_{\delta^*} = 1950$, is used to estimate the influence of the RANS solution on the calculated wall-pressure spectra. The results are compared with experimental data by Schewe [53].

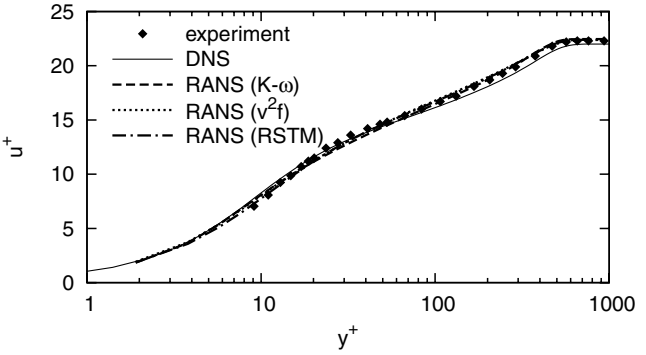

Fig. 4 Flat plate boundary-layer streamwise velocity profiles in wall coordinates. Experiment from Schewe [53]. DNS from Spalart [54].

Steady Flow Solution

RANS computations were run on a highly resolved two-dimensional grid in STAR–CCM+, using the K-ω SST turbulence model and the v^2f model and, in FLUENT, using the RSTM. As shown in Fig. 4, the resolution close to the walls is such that y^+ is less than two. The computed mean velocity profile (Fig. 4) is independent of the chosen turbulence model and agrees very well (maximum deviation is less than 5%) with experimental data and a direct numerical simulation (DNS) with approximately the same Reynolds number [54].

Compared with the mean flow prediction, the correct computation of turbulence data is a much more challenging matter, since the results are very sensitive to the turbulence model used. Furthermore, the wall-pressure model does not require the turbulent kinetic energy, which is computed by most standard turbulence models but uses the vertical velocity fluctuations instead. Thus, the required anisotropy factors $\beta_i(x_2)$ were calculated from the RANS simulation with the RST model.

In Fig. 5, the calculated vertical velocity fluctuations are plotted. The comparison of the different RANS turbulence models with experimental data is satisfactory but not as good as for the mean velocity data. The highest deviation is found for the v^2f model ranging to more than 10%.

The velocity correlation length scale required for wall-pressure calculation is assumed to be directly proportional to the mixing length ($\Lambda = 1.5l_m$), so this is the only parameter to be considered. It depends on the turbulence length scale as $l_m = C_mL$, where C_m depends on the turbulence model.

The mixing length calculated from the different RANS results is shown in Fig. 6. As references, the Prandtl mixing length and the mixing length calculated from the RSTM results with Eq. (7) (solid line) are plotted. Based on these references, the factor C_m was fixed at 1.9 for the K-ω and the RSTM and at 0.65 for the v^2f model. The result is a similar behavior for all turbulence models, with the exception of the result obtained with the $l_m(v^2f)$ model, which does not approach zero close to the wall.

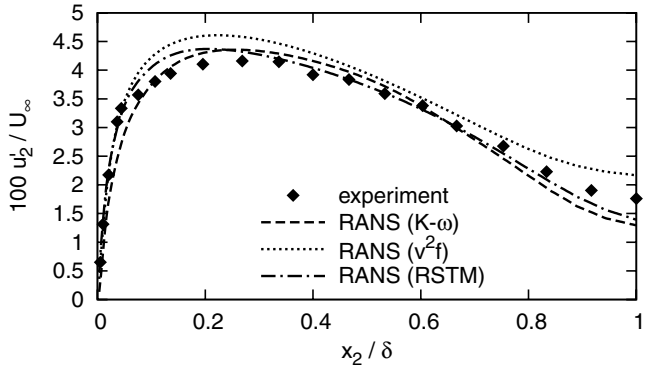

Fig. 5 Vertical velocity fluctuations in a flat plate boundary layer (k-ω: $\bar{u}_2' = \sqrt{2K\beta_2}$; experiment from Schewe [53]: $\bar{u}_2' = \bar{u}_2'\sqrt{\beta_2/\beta_1}$).

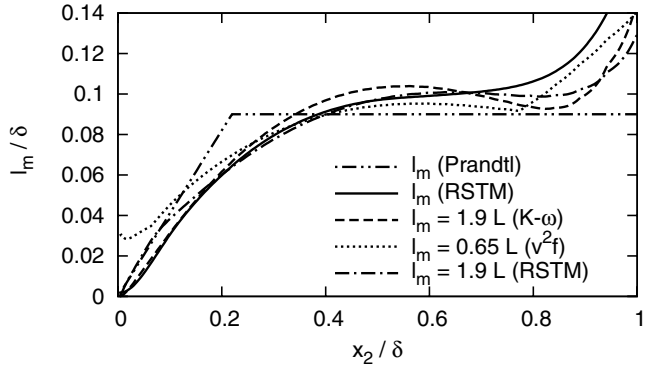

Fig. 6 Mixing length in a flat plate boundary layer.

Wall-Pressure Spectra

Since the flat plate boundary-layer profile is quite different from test case 1, it cannot be expected that the same conditions for the convection velocity are applicable. Therefore, the different models for the convection velocity are tested for the present case as well.

The calculated spectra are plotted together with Schewe's [53] measurements in Fig. 7. As in the preceding section, both axes were made nondimensional with the freestream velocity, the dynamic pressure, and the displacement thickness. None of the empirical parameters were tuned to get the best matching of computational results with the experiment. Instead, analytical model equations from the literature were tested and a choice was made based on the test case with adverse pressure gradient boundary layer. The influence of the three models for U_c on the wall-pressure spectrum is negligible in the low-frequency range up to $\omega\delta^*/U_\infty = 1$, as shown in Fig. 7. At higher frequencies, both models with nonconstant $U_c(k_1)$ still produced roughly the same results, while for the constant U_c, the spectrum was shifted to higher frequencies, closer to the experimental values. Because of this slightly better agreement with experiments and the lower integral error, it was decided to use $U_c = 0.9U_\infty$ for postprocessing of the flat plate data.

For the scale anisotropy factor α, the model presented in Eq. (11) was used again.

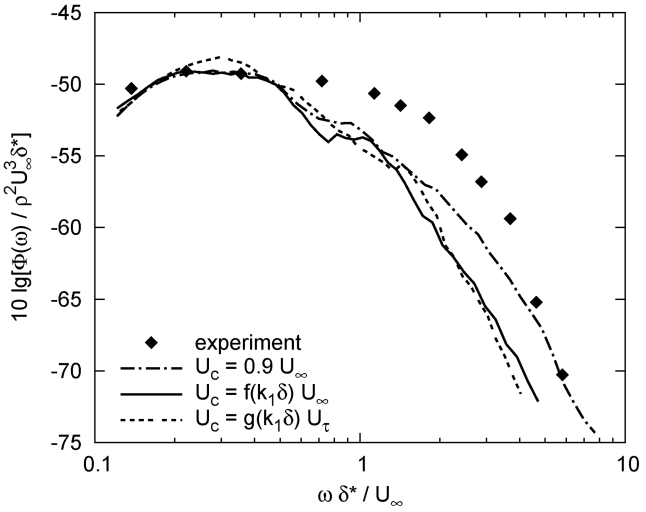

Fig. 7 Wall-pressure spectrum in a flat plate boundary layer, depending on the model for the convection velocity U_c. The RANS solution with RST model was used. Experiment from Schewe [53].

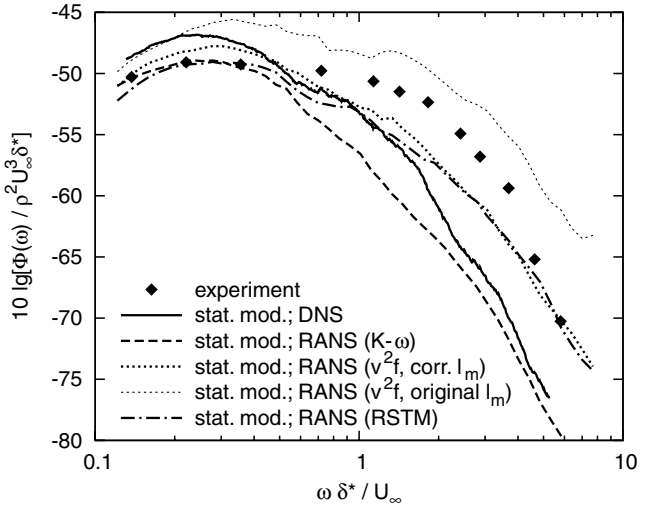

Fig. 8 Wall-pressure spectrum in a flat plate boundary layer for different RANS input data sets. Experiment from Schewe [53]. DNS from Spalart [54].

Having decided on all submodels, the wall-pressure spectrum was calculated based on the flowfield results from the different turbulence models. The results are shown in Fig. 8. For the v^2f model, the mixing length close to the wall was limited by the Prandtl approach as

$$l_m = \min(l_{m,v^2f}, \kappa x_2) \tag{15}$$

because the calculated amplitudes were significantly higher than for all other models. The spectra with and without this correction are both plotted in Fig. 8.

The predictions of wall pressure in the low-frequency range are for all models within a band of 3 dB, which includes the experimental points. For $\omega\delta^*/U_\infty > 0.5$, the predicted falloff is more rapid than the measured one for all models, and the results from the different turbulence models differ more from each other. For all computations, the integrated pressure fluctuation $\langle p^2 \rangle = \int \Phi(\omega)\, \mathrm{d}\omega$ is thus lower than the experimental value (DNS: 2.2 dB, K-ω: 4.4 dB, v^2f: 1.5 dB, RSTM: 2.5 dB). The figure clearly shows that spectra calculated with the statistical model strongly depend on the input flowfield information. Changing the turbulence model will have a strong influence on the spectral shape of the calculated wall pressure. Furthermore, it appears that the statistical model does a good job in the low-frequency range, while it underpredicts the high-frequency fluctuations.

Application to Valeo Controlled-Diffusion Airfoil

Available Experimental Data

The case of a Valeo CD airfoil at an 8° angle of attack was studied experimentally in the anechoic wind tunnel at ECL [24] and in the turbulent shear flow laboratory at Michigan State University (MSU) [55]. The facility at MSU was modified carefully to match the conditions at ECL as closely as possible. The airfoil mockup had a constant chord length of $c = 134$ mm and a span of $b = 300$ mm. It was held between two horizontal side plates fixed to the nozzle of the open-jet wind tunnel, as shown in Fig. 9a. These plates were 250 mm ($\approx 1.85c$) apart, and the width of the rectangular jet was 500 mm ($\approx 3.7c$). As shown by Moreau et al. [38], this setup insured that the influence of the side plates on the flow in the airfoil midspan plane was minimized. All tests were run with a reference velocity of $U_{\mathrm{ref}} = 16$ m/s, which corresponds to a Reynolds number (based on the airfoil chord length) of $Re_c = 1.6 \cdot 10^5$.

The CD airfoil mockup was equipped at midspan with 21 flush-mounted remote Electret microphone probes (RMPs) [1]. The RMPs measured both the mean and fluctuating pressure within a frequency range of 20–25 kHz. Figure 9b shows the layout of the streamwise RMPs at the midspan plane of the CD airfoil. Details of the wall-pressure measurements in this configuration can be found in Moreau and Roger [25]. The far-field noise was measured using a single Brüel and Kjaer 12.7 mm (0.5 in.) Type-4181 microphone located in the midspan plane of the airfoil at a distance of 2 m from the airfoil trailing edge. The RMP and microphone measurements were acquired simultaneously. Furthermore, hot-wire measurements were performed in the wake of the airfoil and in the suction side boundary layer to characterize the flowfield in terms of mean velocity and fluctuations. The boundary-layer measurements were performed on lines perpendicular to the local curvature at the positions of the RMPs.

Steady Flow Computation

Numerical Setup

To obtain reliable results in the boundary layer of the airfoil, it was necessary to reproduce the experimental blade loading as closely as possible. In fact, as Moreau et al. [38] showed, it is not possible to simply use a uniform inflow condition corresponding to a jet of infinite extension. The actual behavior of the airfoil in the narrow jet is more similar to the one in a cascade. Thus, the whole setup, including airfoil, wind-tunnel nozzle, and free space, had to be included in the simulation. On the other hand, a high resolution of the region near the airfoil was necessary to resolve the boundary layer sufficiently. An existing RANS simulation of Moreau et al. [38], which included the whole wind-tunnel setup, was used to provide realistic boundary conditions for a high-resolution computation of the area close to the airfoil. The two-dimensional domain of Moreau et al. [38] had 85,560 elements and extended 8 chord lengths upstream from the airfoil, 26 chord lengths downstream, and 44 chord lengths in the normal direction. The velocity information was extracted from this simulation on a c-shaped line, as sketched in Fig. 10, and used as the inlet condition for a second RANS simulation on a smaller domain but with a finer grid. The grid for the second RANS simulation is sketched in Fig. 11. It was a two-dimensional cut from a LES grid [26], with a spanwise extend of 0.1 chord length, and the number of cells in this direction was 64, so the total number of cells amounted to $5.2 \cdot 10^6$. The RANS computations were performed on a 81,000-cell grid, extending 4 chord lengths in the streamwise direction and 2 chord lengths in the normal direction. The resolution close to the walls was approximately $y^+ = 1$.

The flowfield was computed in STAR-CCM+, using the K-ω SST turbulence model and the v^2f model, and the computation using the RSTM was run in FLUENT. For the RSTM computation, enhanced wall treatment was chosen, which is adapted to a resolved viscous sublayer. Pressure gradient effects were taken into account for the wall treatment.

Comparison of Steady Flow Results

The pressure coefficient $c_p = (p - p_\infty)/q_\infty$ on the airfoil surface was available from the experiments of Moreau and Roger [25]. It is shown in Fig. 12, together with the results of the different RANS computations and of the LES computation in the same configuration [47]. The complex flow pattern at the leading edge includes a laminar separation and reattachment then transition to turbulence and, finally, the development of a turbulent boundary layer. At the leading edge, the computed pressure distribution strongly depends on the turbulence model, and none of them agrees well with the experimental values. The same behavior has been observed in LES

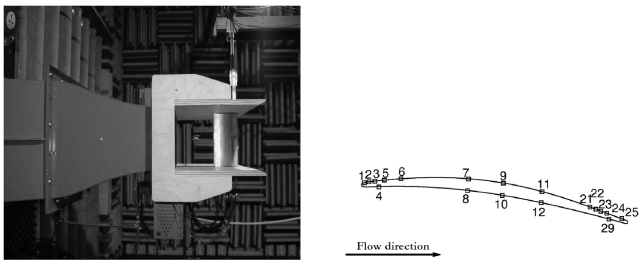

a) Wind tunnel set-up at ECL **b) CD airfoil with remote microphone positions**

Fig. 9 Experimental configuration.

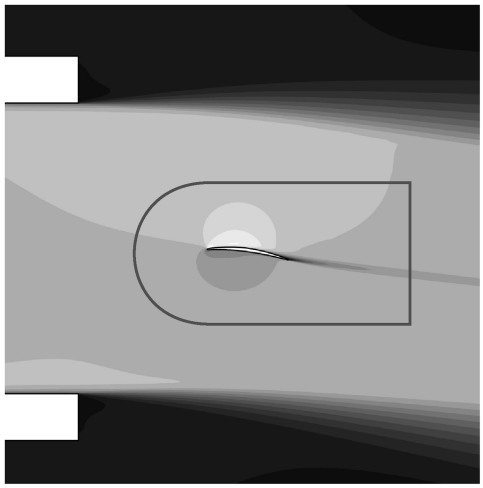

Fig. 10 Velocity contours calculated by complete RANS; the domain of the higher-resolved RANS is indicated by the solid line.

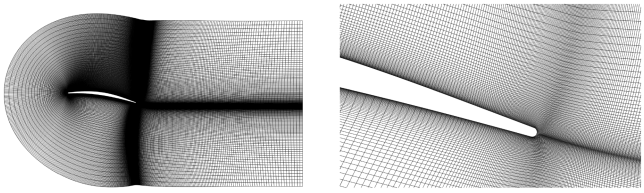

a) Complete domain **b) Zoom at the trailing edge**

Fig. 11 Computational mesh for RANS simulations.

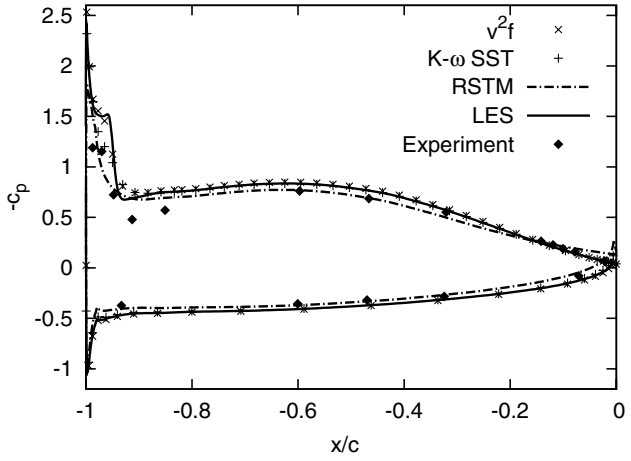

Fig. 12 Pressure coefficient on the CD airfoil. Experiment from Moreau and Roger [25]. LES from Christophe et al. [47].

computations, the size of the recirculation being affected by the code and the subgrid scale models used [47,56]. The LES captures the boundary-layer transition on the suction side, which is triggered by an unsteady laminar separation near the leading edge, whereas the RANS simulations produce too much turbulence to yield the proper recirculation bubble. This could not be predicted by either of the RANS models, since no transition modeling was included in the simulations. On the other hand, the pressure distribution near the trailing edge is well predicted by all RANS and LES computations. Both two-equation models agree almost perfectly there, and the RSTM differs a little from the two former, but the agreement with the experiments is also good.

The boundary layer was analyzed at $x/c = -0.023$ (corresponds to position 25 in Fig. 9b) at the suction side of the airfoil close to the trailing edge. The flow data were extracted on a profile perpendicular to the local airfoil surface, with a grid resolution of $\Delta x_2 = 33\ \mu$m. The maximum velocity in the extracted data set was assumed to be equal to the freestream velocity U_∞.

The integral boundary-layer data are summarized in Table 1. Hot-wire measurements were performed by Moreau et al. [24,55], and the LES data are from Christophe et al. [47]. The boundary-layer thickness predicted by both two-equation turbulence models matches the experimental value within an acceptable error, while the RSTM calculations strongly overpredict the boundary-layer thickness. Since the RSTM computation was run in FLUENT while the others were run in STAR-CCM+, it was not completely clear if the strong differences were due to the turbulence modeling or to the code.

Table 1 Integral boundary-layer data at position 25 on the suction side of the CD airfoil, near the trailing edge[a,b]

	Exp.	v^2f	K-ω	RSTM	LES
δ^*, mm	1.83	2.04	2.17	2.86	2.28
δ_{99}, mm	5.36	6.54	6.61	8.38	6.48
U_∞ m/s	16.09	16.87	16.76	16.78	16.79
Re_{δ^*}	2197	2568	2714	3581	2857

[a]Experiment from Moreau et al. [55].
[b]LES from Christophe et al. [47].

A comparative computation in FLUENT with the K-ω SST turbulence model and the same solver setup suggests that differences are most probably due to turbulence modeling. The differences in velocity profile between the K-ω computations in STAR-CCM+ and FLUENT were negligible. Furthermore, different wall treatment methods were applied, but all of them yielded either a velocity profile still further away from the experiment and the other computations or no convergent solution could be found at all.

The mean velocity profiles at position 25 are plotted in Fig. 13. Also, from this figure, it is quite obvious that the RSTM results strongly differ from experiment and LES data; neither the profile shape nor the integral values are correct. The RSTM results, as they are obtained, are not usable for the statistical model regarding the large discrepancies when compared with other RANS computations and experiments. Thus, they are not considered in the following sections.

The two other models behave quite similar to each other and both predict well the velocity profile. The v^2f model is a bit better in the region close to the wall; in the outer region, both results match very closely. The mean flow prediction can be regarded as sufficiently exact for statistical wall-pressure modeling.

For obtaining the vertical velocity fluctuations from the isotropic K-ω computation and from the experiments (just streamwise fluctuations were available), the anisotropy factors $\beta_{1,2}(x_2/\delta)$ from the flat plate computations were used. This might not be an optimal choice since, in the present case, the boundary-layer profile is different, but better data were not available because the RSTM data were unusable. The wall-normal velocity fluctuations (Fig. 14) are underpredicted by the K-ω and v^2f models, but at least the peak is roughly at the correct wall distance. For comparison, the LES profile is also plotted in the same figure, showing a better agreement with experiments when compared with RANS computations. The amplitude of the wall-normal velocity fluctuations is almost correctly reproduced, but the maximum peak is slightly shifted to the near-wall region when compared with experiments and RANS computations.

Finally, the mixing length was also calculated according to Eqs. (8) and (10) (Fig. 15) using the same factors C_m as in the validation section. The mixing length calculated from the K-ω results is systematically smaller than the one from the v^2f computations and, in the freestream, they even show different trends. For a rough comparison, the Prandtl mixing length based on the experimental boundary-layer thickness and the one calculated from the LES computation are also plotted. Again, the v^2f mixing length will be limited for acoustical postprocessing by the Prandtl approach [Eq. (15)].

Wall-Pressure Spectra

Wall-pressure spectra were calculated for 1000 frequencies and 3000 random data sets per frequency and using Eqs. (11) and (13) for the scale anisotropy and the convection velocity, respectively.

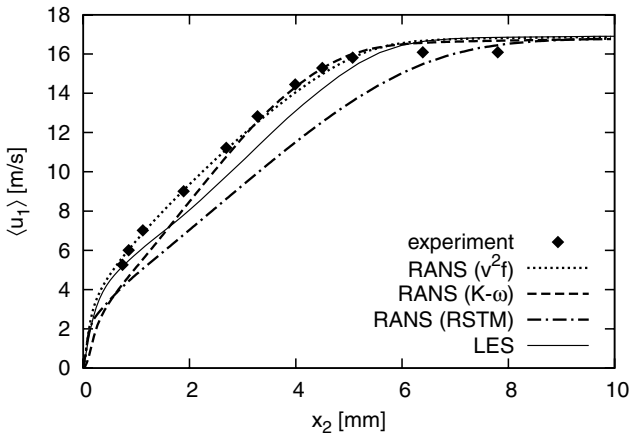

Fig. 13 Mean velocity profile in the boundary layer near trailing edge ($x/C = -0.023$). Experiment from Moreau et al. [55]. LES from Christophe et al. [47].

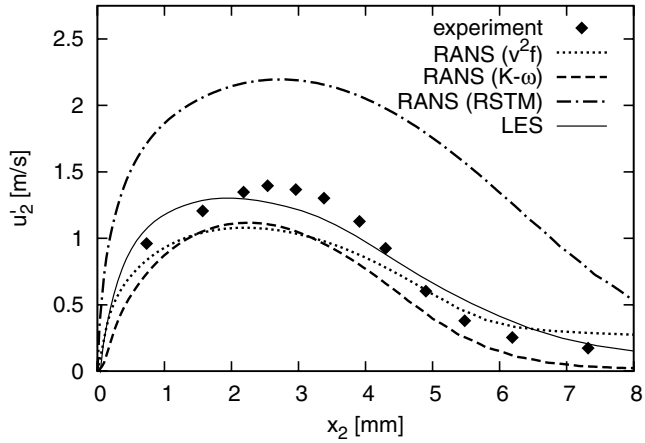

Fig. 14 Vertical velocity fluctuations in the boundary layer near trailing edge ($x/C = -0.023$). Experiment from Moreau et al. [55]. LES from Christophe et al. [47].

The calculated spectra for position 25 close to the trailing edge are shown in Fig. 16. The plotted experimental spectrum was measured by Moreau et al. [24]. Two spectra from LESs are plotted as well: one by Wang et al. [26] and one by Christophe et al. [47].

If the hot-wire data [24] are used as input for the statistical wall-pressure model (solid line), the spectrum is overpredicted in the midfrequency range when compared with the measured spectrum (integral error +2.9 dB), but the agreement with both LES spectra in this range is good. For the RANS flowfield (v_2f), the overprediction is lower (integral error +0.6 dB), but the agreement with the experiment in the low-frequency range is not as good (underprediction up to 5 dB below 300 Hz). Using the K-ω data yields a spectrum at too low a level for all frequencies (integral error −4.8 dB), which is most probably due to the lower-velocity gradient close to the wall and the lower mixing length.

Altogether, the combination of the RANS v_2f solution and the statistical wall-pressure model yields a satisfyingly accurate spectrum, which agrees as well with experiments as the LES results do. By contrast, the calculation based on the K-ω results only predicts correct trends in the spectrum but fails in terms of absolute spectral level.

Emitted Sound

The radiated sound from the airfoil was calculated by means of Amiet's [19] theory. The results for a receiver at $R_r = 2$ m, $\theta_r = 90°$ are shown in Fig. 17. The differences between the three calculated far-field sound spectra are basically the same as in the wall-pressure spectra, so differences in wall-pressure spectra are translated directly into differences in sound spectra. The K-ω flowfield results in an underestimation at all frequencies; with v_2f, the prediction is

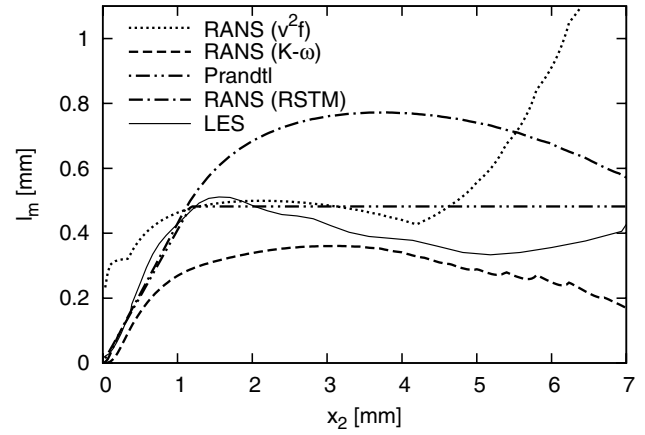

Fig. 15 Mixing length in the boundary layer near trailing edge ($x/C = -0.023$). LES from Christophe et al. [47].

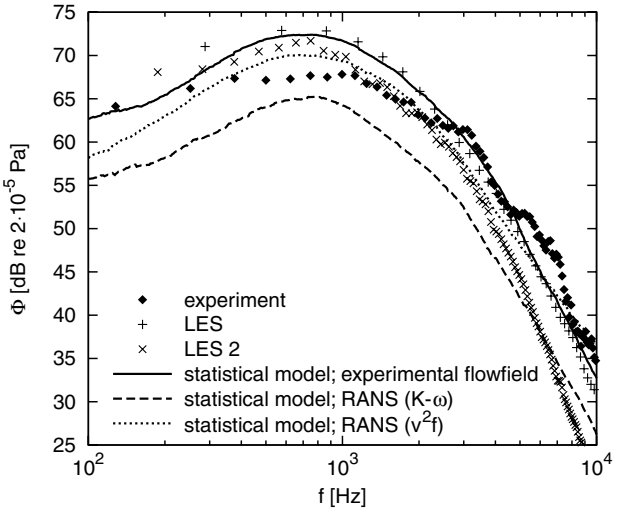

Fig. 16 Wall-pressure spectrum near trailing edge. Experiment from Moreau et al. [24]. LES from Christophe et al. [47]. LES 2 from Wang et al. [26].

comparatively good. Statistical model and LES computations have similar trends, which is an acceptable prediction beyond 1 kHz and an overestimation of the emitted sound below this limit.

Unfortunately, there are no sound measurement data available for the low- and high-frequency range due to a very low signal-to-noise ratio in these regions, so it cannot be judged whether the statistical model results are better than the LES spectra or vice versa. Anyway, it can be concluded that it is possible to use the chain RANS (v_2f), statistical model, Amiet's [19] theory to calculate the trailing-edge noise of an airfoil with reasonable accuracy. Compared with LES, the quality of the computed spectra is similar, but the computational costs are much lower.

Computational Costs

To emphasize the potential of a RANS solution together with the statistical model for the saving of computational resources when compared with LES, the according computational times are listed in Table 2. The underlying RANS computation of the complete setup, including the nozzle, is the same for both methods, and the same applies to the sound computation with Amiet's [19] theory, which needs less than 10 s per computation. These two steps need not be considered in the comparison.

The computational time for the RANS solution was 2:05 h for the K-ω model (8000 iterations), 2:45 h for the v^2f model (7000

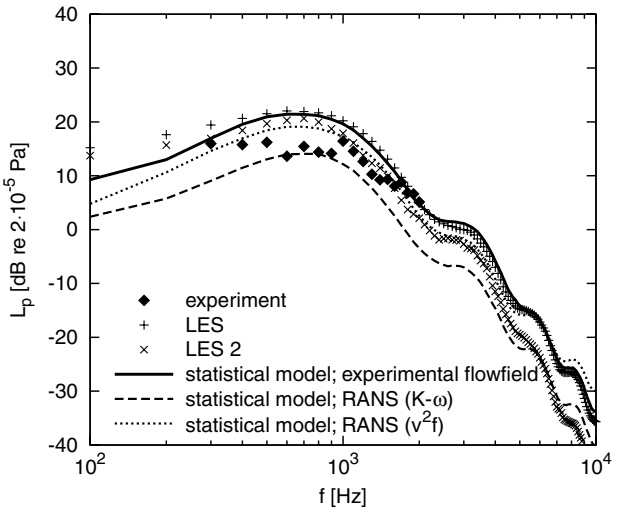

Fig. 17 Far-field acoustic spectra on the midspan plane above the CD airfoil in a distance of 2 m. Experiment from Moreau et al. [24]. LES from Christophe et al. [47]. LES 2 from Wang et al. [26].

Table 2 Comparison of computational costs for RANS and LES solutions

	RANS	LES
Grid size/number of cells	81,000	5.2 million
CPU time for flow computation	2, . . . , 10 h	32,000 h
CPU time for spectral model	<2 min	——
Total duration of computations	<10 m	82 days

iterations), and approximately 10 h for the RSTM (35,000 iterations) on an Intel Pentium 4 CPU (3.4 GHz). Compared with this, the calculation of the wall-pressure spectrum with the spectral model at one point is practically negligible; it was done in 85 s. The maximum total CPU time required is, hence, about 10 h.

The LES [47] did not require the postprocessing step, but the costs for the flow computation itself were already by orders of magnitude higher. The LES was run parallel on 16 processors. The time to compute one nondimensional time $\tau_{nd} = tU_\infty/c = 1$ was about 200 h. To remove the transient part from the computation took $\tau_{nd} = 5$ and, to obtain converged flow statistics, another $\tau_{nd} = 5$. So, in total, about 32,000 CPU h were necessary to compute the wall-pressure spectra. Compared with this, the costs and waiting time of the RANS solution are negligible.

Conclusions

A method for calculation of the trailing-edge noise of an airfoil based on a steady RANS solution of the flowfield was successfully applied. It includes a statistical model available in the literature to compute a wall-pressure spectrum beneath a turbulent boundary layer and a calculation of radiated far-field sound with Amiet's [19] theory of airfoil noise. The statistical model for wall-pressure fluctuations was first validated with two test cases from the literature, a boundary layer with adverse pressure gradient, and a flat plate boundary layer without pressure gradient. The influence of the choice of the model for the convection velocity was found to be minor. For a second parameter of the statistical model, the turbulence scale anisotropy factor α, a simple model based on the nondimensional wave length, was proposed, which produces good results for all tested cases. The method was then applied to the case of a Valeo CD airfoil placed in a jet wind tunnel in the anechoic facility of ECL. The wall-pressure spectrum calculated on basis of the v^2f results agreed well with an experimental spectrum and two spectra obtained from different LES. The K-ω SST flowfield produced a wall-pressure spectrum with a similar shape as the former one but underpredicted the experimental spectrum by roughly 5 dB. The radiated noise from the airfoil trailing edge was computed based on these wall-pressure spectra using Amiet's theory. The agreement with far-field microphone measurement was good, and the best agreement could be achieved with the v^2f solution. The proposed method is therefore shown to work for both canonical flows and a more practical application, and the associated costs are strongly reduced when compared with LES.

The statistical model is, however, limited to boundary layers with small gradients in streamwise and spanwise directions and is not applicable in separated flow regions. Other limitations for the practical use of the statistical model are the empirical factors, which are not shown to be universal, as well as the best choice of turbulence model in the RANS solution. The v^2f turbulence model has the advantage that it directly provides information about the wall-normal velocity fluctuations required for the spectral model. A possible improvement of the method would be to incorporate more sophisticated methods of decomposition of the computed turbulent kinetic energy into Reynolds stresses, as proposed by Guo and Chang [57].

Even though the acoustical postprocessing of the calculated wall-pressure spectra was presently restricted to a trailing-edge noise computation with Amiet's [19] theory, the method can be easily extended to other acoustic analogies, such as Curle [17] or Ffowcs Williams and Hawkings [18]. For this purpose, the boundary-layer profiles have to be extracted at several positions from the RANS solution, and the statistical model is used to compute a surface distribution of pressure fluctuations in the frequency domain. Moreover, the present method only works for RANS computations with a high resolution of the boundary layer (i.e. $y^+ \leq 1$). Indeed, it would be desirable to extend the applicability to coarse meshes, which use wall functions, since this approach is widely used in complex three-dimensional geometries. For this purpose, wall functions have to be implemented directly into the statistical model to use the correct velocity gradient and turbulent fluctuations close to the wall.

Acknowledgments

J. Christophe has been supported by a fellowship from the Fond pour la Formation à la Recherche dans l'Industrie et dans l'Agriculture. The present research was carried out during the von Karman Institute (VKI) Diploma Course 2008/09 under a fellowship of the VKI and the German Bundeswehr. The acoustical data were provided by Michel Roger (École Centrale de Lyon, France) and Stéphane Moreau (Université de Sherbrooke, Canada), and the hot-wire measurements on the controlled-diffusion airfoil were carried out by Douglas Neal at Michigan State University.

References

[1] Pèrennès, S., and Roger, M., "Aerodynamic Noise of a Two-Dimensional Wing with Highlift Devices," 4th AIAA/CEAS Aeroacoustics Conference Meeting, AIAA Paper 1998-2338, 1998.

[2] Singer, B. A., Lockard, D. P., and Brentner, K. S., "Computational Aeroacoustic Analysis of Slat Trailing-Edge Flow," *AIAA Journal*, Vol. 38, No. 9, 2000, pp. 1558–1564. doi:10.2514/2.1177

[3] Sharland, I. J., "Sources of Noise in Axial Flow Fans," *Journal of Sound and Vibration*, Vol. 1, No. 3, 1964, pp. 302–322. doi:10.1016/0022-460X(64)90068-9

[4] Envia, E., Wilson, A. G., and Hu, D. L., "Fan Noise: A Challenge to CAA," *International Journal of Computational Fluid Dynamics*, Vol. 18, No. 6, 2004, pp. 471–480. doi:10.1080/10618560410001673489

[5] Caro, S., and Moreau, S., "Aeroacoustic Modeling of Low Pressure Axial Flow Fans," 6th AIAA/CEAS Aeroacoustics Conference, AIAA Paper 2000-2094, 2000.

[6] Hubbard, H. H., and Shepherd, K. P., "Aeroacoustics of Large Wind Turbines," *Journal of the Acoustical Society of America*, Vol. 89, No. 6, 1991, pp. 2495–2507. doi:10.1121/1.401021

[7] Prospathopoulos, J. M., and Voutsinas, S. G., "Noise Propagation Issues in Wind Energy Applications," *Journal of Solar Energy Engineering*, Vol. 127, No. 2, 2005, pp. 234–241. doi:10.1115/1.1862257

[8] Zhu, W. J., Heilskov, N., Shen, W. Z., and Sorensen, J. N., "Modeling of Aerodynamically Generated Noise from Wind Turbines," *Journal of Solar Energy Engineering*, Vol. 127, No. 4, 2005, pp. 517–528. doi:10.1115/1.2035700

[9] Hoover, R. M., and Blazier, W. E., "Noise Control in Heating, Ventilating, and Air-Conditioning Systems," *Handbook of Acoustical Measurements and Noise Control*, Acoustical Society of America, Melville, NY, 1998, Chap. 42.

[10] Iqbal, M. A., Willson, T. K., and Thomas, R. J., *Control of Noise in Ventilation Systems: A Designers' Guide*, Spon, London, 1977.

[11] Madani, V., and Ziada, S., "Aeroacoustic Characteristics of Automotive HVAC Systems," Society of Automotive Engineers SP 2158, Warrendale, PA, 2008.

[12] Schram, C., and Desmet, W., "Interfacing a Boundary Element Method with Low-Order CFD and Automotive Examples," *Computational Aeroacoustics*, VKI Lecture Series, Vol. 2006-05, Von Karman Inst. for Fluid Dynamics, Rhode-St-Genese, Belgium, 2006.

[13] George, A. R., "Automobile Aerodynamic Noise," *1990 SAE International Congress and Exposition*, Society of Automotive Engineers Paper 900315, Warrendale, PA, Feb. 1990.

[14] Parchen, R., "Aerodynamic Noise of Aircraft and Road Vehicles," *Advances in Aeroacoustics and Applications*, VKI Lecture Series, Vol. 2004–05, Von Karman Inst. for Fluid Dynamics, Rhode-St-Genese, Belgium, 2004.

[15] Lighthill, M. J., "On Sound Generated Aerodynamically. Part I. General Theory," *Proceedings of the Royal Society of London, Series A:*

Mathematical and Physical Sciences, Vol. 211, No. 1107, 1952, pp. 564–587.
doi:10.1098/rspa.1952.0060

[16] Lighthill, M. J., "On Sound Generated Aerodynamically. Part II. Turbulence as a Source of Sound," *Proceedings of the Royal Society of London, Series A: Mathematical and Physical Sciences*, Vol. 222, No. 1148, 1954, pp. 1–32.
doi:10.1098/rspa.1954.0049

[17] Curle, N., "The Influence of Solid Boundaries upon Aerodynamic Sound," *Proceedings of the Royal Society of London, Series A: Mathematical and Physical Sciences*, Vol. 231, No. 1187, 1955, pp. 505–514.
doi:10.1098/rspa.1955.0191

[18] Ffowcs Williams, J. E., and Hawkings, D. L., "Sound Generation by Turbulence and Surfaces in Arbitrary Motion," *Philosophical Transactions of the Royal Society of London, Series A: Mathematical and Physical Sciences*, Vol. 264, No. 1151, 1969, pp. 321–342.
doi:10.1098/rsta.1969.0031

[19] Amiet, R. K., "Acoustic Radiation from an Airfoil in a Turbulent Stream," *Journal of Sound and Vibration*, Vol. 41, No. 4, 1975, pp. 407–420.
doi:10.1016/S0022-460X(75)80105-2

[20] Roger, M., and Moreau, S., "Broadband Self-Noise from Loaded Fan Blades," *AIAA Journal*, Vol. 42, No. 3, 2004, pp. 536–544.
doi:10.2514/1.9108

[21] Roger, M., and Moreau, S., "Back-Scattering Correction and Further Extensions of Amiet's Trailing-Edge Noise Model. Part 1: Theory," *Journal of Sound and Vibration*, Vol. 286, No. 3, 2005, pp. 477–506.
doi:10.1016/j.jsv.2004.10.054

[22] Roger, M., Moreau, S., and Wang, M., "An Analytical Model for Predicting Airfoil Self-Noise Using Wall-Pressure Statistics," *Annual Research Briefs 2002*, Center for Turbulence Research, Stanford, CA, 2002, pp. 405–414.

[23] Christophe, J., Anthoine, J., and Moreau, S., "Amiet's Theory in Spanwise-Varying Flow Conditions," *AIAA Journal*, Vol. 47, No. 3, 2009, pp. 788–790.
doi:10.2514/1.37502

[24] Moreau, S., Neal, D., Khalighi, Y., Wang, M., and Iaccarino, G., "Validation of Unstructured-Mesh LES of the Trailing-Edge Flow and Noise of a Controlled-Diffusion Airfoil," *Proceedings of the Summer Program 2006*, Center for Turbulence Research, Stanford, CA, 2006, pp. 1–14.

[25] Moreau, S., and Roger, M., "Effect of Airfoil Aerodynamic Loading on Trailing-Edge Noise Sources," *AIAA Journal*, Vol. 43, No. 1, 2005, pp. 41–52.
doi:10.2514/1.5578

[26] Wang, M., Moreau, S., Iaccarino, G., and Roger, M., "Les Prediction of Pressure Fluctuations on a Low Speed Airfoil," *Annual Research Briefs*, Center for Turbulence Research, Stanford, CA, 2004.

[27] Moreau, S., Henner, M., Casalino, D., Gullbrand, J., Icarino, G., and Wang, M., "Toward the Prediction of Low-Speed Fan Noise," *Proceedings of the Summer Program 2006*, Center for Turbulence Research, Stanford, CA, 2006, pp. 519–531.

[28] Kraichnan, R. H., "Pressure Fluctuations in Turbulent Flow Over a Flat Plate," *Journal of the Acoustical Society of America*, Vol. 28, No. 3, 1956, pp. 378–390.
doi:10.1121/1.1908336

[29] Lilley, G. M., and Hodgson, T. H., "On Surface Pressure Fluctuations in Turbulent Boundary Layers," AGARD Note 101, 1960.

[30] Lilley, G. M., "Pressure Fluctuations on an Incompressible Turbulent Boundary Layer," AGARD Rept. 133, 1960.

[31] Panton, R. L., and Linebarger, J. H., "Wall Pressure Spectra Calculations for Equilibrium Boundary Layers," *Journal of Fluid Mechanics*, Vol. 65, No. 2, 1974, pp. 261–287.
doi:10.1017/S0022112074001388

[32] Lee, Y., Blake, W. K., and Farabee, T. M., "Modeling of Wall Pressure Fluctuations Based on Time Mean Flow Field," *Journal of Fluids Engineering*, Vol. 127, No. 2, 2005, pp. 233–240.
doi:10.1115/1.1881698

[33] Farabee, T. M., and Casarella, M. J., "Spectral Features of Wall Pressure Fluctuations Beneath Turbulent Boundary Layers," *Physics of Fluids A*, Vol. 3, No. 10, 1991, pp. 2410–2420.
doi:10.1063/1.858179

[34] Rozenberg, Y., Roger, M., and Moreau, S., "Fan Blade Trailing-Edge Noise Prediction Using RANS Simulations," *Acoustics '08*, Acoustical Soc. of America, Melville, NY, 2008, pp. 5207–5212.

[35] Glegg, S., Morin, B., Atassi, O., and Reba, R., "Using RANS Calculations of Turbulent Kinetic Energy to Provide Predictions of Trailing Edge Noise," 14th AIAA/CEAS Aeroacoustics Conference, AIAA 2008-2993, 2008.

[36] Bèchara, W., Bailly, C., Lafon, P., and Candel, S. C., "Stochastic Approach to Noise Modeling for Free Turbulent Flows," *AIAA Journal*, Vol. 32, No. 3, 1994, pp. 455–463.
doi:10.2514/3.12008

[37] Golliard, J., van Lier, L., and Vedy, E., "Generation of Unsteady Aeroacoustic Source Terms from Steady CFD," *Computational Aeroacoustics*, VKI Lecture Series, Vol. 2006–5, Von Karman Inst. for Fluid Dynamics, Rhode-St-Genese, Belgium, 2006.

[38] Moreau, S., Henner, M., Iaccarino, G., Wang, M., and Roger, M., "Analysis of Flow Conditions in Freejet Experiments for Studying Airfoil Self Noise," *AIAA Journal*, Vol. 41, No. 10, 2003, pp. 1895–1905.
doi:10.2514/2.1905

[39] Moreau, S., Mendonca, F., Qazi, O., Prosser, R., and Laurence, D., "Influence of Turbulence Modelling on Airfoil Unsteady Simulations of Broadband Noise Sources," 11th AIAA/CEAS Aeroacoustics Conference Meeting and Exhibit, AIAA Paper 2005-2916, 2004.

[40] "STAR–CCM+ User Guide," Ver. 3.04.008, CD-adapco, Inc.,, New York, 2008.

[41] "FLUENT User's Guide," Ver. 6.3.26., FLUENT, Inc., Lebanon, NH, 2006

[42] Wilcox, D. C., *Turbulence Modeling for CFD*, DCW Industries, La Cañada, CA, 1998.

[43] Menter, F. R., "Two-Equation Eddy-Viscosity Turbulence Modeling for Engineering Applications," *AIAA Journal*, Vol. 32, No. 8, 1994, pp. 1598–1605.
doi:10.2514/3.12149

[44] Durbin, P. A., "Near-Wall Turbulence Closure Modelling Without 'Damping Functions'," *Theoretical and Computational Fluid Dynamics*, Vol. 3, No. 1, 1991, pp. 1–13.
doi:10.1007/BF00271513

[45] Durbin, P. A., "Separated Flow Computations with the $k-\varepsilon-v^2$ Model," *AIAA Journal*, Vol. 33, No. 4, 1995, pp. 659–664.
doi:10.2514/3.12628

[46] Thakur, S., and Shyy, W., "Reynolds Stress Models for Flows in Complex Geometries: Review and Application," 30th AIAA Fluid Dynamics Conference, AIAA Paper 1999-3782, 1999–3782.

[47] Christophe, J., Anthoine, J., and Moreau, S., "Trailing Edge Noise of a Controlled-Diffusion Airfoil at Moderate and High Angle Of Attack," 15th AIAA/CEAS Aeroacoustics Conference, AIAA Paper 2009-3196, 2009.

[48] Caisch, R. E., "Monte Carlo and Quasi-Monte Carlo Methods," *Acta Numerica*, Vol. 7, 1998, pp. 1–49.
doi:10.1017/S0962492900002804

[49] Klebanoff, P. S., "Characteristics of Turbulence in a Boundary Layer with Zero Pressure Gradient," NACA TN 3178, 1954.

[50] Amiet, R. K., "Noise due to Turbulent Flow Past a Trailing Edge," *Journal of Sound and Vibration*, Vol. 47, No. 3, 1976, pp. 387–393.
doi:10.1016/0022-460X(76)90948-2

[51] Bradshaw, P., "The Turbulence Structure of Equilibrium Boundary Layers," *Journal of Fluid Mechanics*, Vol. 29, No. 4, 1967, pp. 625–645.
doi:10.1017/S0022112067001089

[52] Wills, J. A. B., "Measurements of the Wave-Number/Phase Velocity Spectrum of Wall Pressure Beneath a Turbulent Boundary Layer," *Journal of Fluid Mechanics*, Vol. 45, No. 1, 1971, pp. 65–90.
doi:10.1017/S0022112071003008

[53] Schewe, G., "On the Structure and Resolution of Wall-Pressure Fluctuations Associated with Turbulent Boundary-Layer Flow," *Journal of Fluid Mechanics*, Vol. 134, 1983, pp. 311–328.
doi:10.1017/S0022112083003389

[54] Spalart, P. R., "Direct Simulation of a Turbulent Boundary Layer up to $R_\theta = 1410$," *Journal of Fluid Mechanics*, Vol. 187, 1988, pp. 61–98.
doi:10.1017/S0022112088000345

[55] Moreau, S., Neal, D., and Foss, J., "Hot Wire Measurements Around a Controlled Diffusion Airfoil in an Open-jet Anechoic Wind Tunnel," *Journal of Fluids Engineering*, Vol. 128, No. 4, 2006, pp. 699–706.
doi:10.1115/1.2201644

[56] Moreau, S., Roger, M., and Christophe, J., "Flow Features and Self-Noise if Airfoils Near Stall or in Stall," 15th AIAA/CEAS Aeroacoustics Conference, AIAA Paper 2009-3198, 2009.

[57] Guo, Y., and Chang, K. C., "On the Calculation of Reynolds Stresses by CFD," 35th AIAA Fluid Dynamics Conference, AIAA Paper 2005-5293, 2005.

A. Lyrintzis
Associate Editor